ORNL/LTR-2016/549

OAK RIDGE NATIONAL LABORATORY
MANAGED BY UT-BATTELLE FOR THE US DEPARTMENT OF ENERGY

Light Water Reactor Sustainability Program:

Study of High Fluence Radiation-induced Swelling and Hardening under Light Water Reactor Conditions

Stanislav I. Golubov[1], Alexander V. Barashev[1,2], and Roger E. Stoller[1]
[1]Oak Ridge National Laboratory
[2]University of Tennessee

Performance Milestone M2LW-16OR0402042

September 2016

Study of High Fluence Radiation-induced Swelling and Hardening under Light Water Reactor Conditions

Stanislav I. Golubov[1], Alexander V. Barashev[1,2], and Roger E. Stoller[1]

[1]Materials Science and Technology Division Oak Ridge National Laboratory Oak Ridge, TN 37831-6114, USA

[2]Center for Materials Processing Department of Materials Science and Engineering University of Tennessee, Knoxville, TN 37996-0750, USA

Prepared for:

Light Water Reactor Sustainability Program Office of Nuclear Energy, Science and Technology U.S. Department of Energy

September 2016
Oak Ridge National Laboratory

Abstract

This report documents a comprehensive model that has been developed to enable simulations of microstructural evolution under the irradiation conditions typical of light water reactor (LWR) internal components. The model, which accounts cascade production of point defects and vacancy, interstitial faulted dislocation loops, interstitial clusters migrating one-dimensionally and the evolution of the network dislocation structure, has been parameterized to account damage accumulation in austenitic stainless steels. Nucleation and growth of an ensemble of cavities is based on accounting the residual and produced by irradiation He atoms and existence of the dislocation and production biases. Additional applications and potential future developments for the model are also discussed.

1. Introduction

The overall objective of this report is to develop a predictive model that can be used in lifetime assessments of these components. This is relevant to component lifetime in the nominal initial license period of about 40 years and is particularly important for considering the extended licensing periods of interest to the Light Water Reactor Sustainability (LWRS) program. The data generated and mechanistic studies will be used to identify key operational limits (if any) to minimize swelling concerns, optimize inspection and maintenance schedules to the most susceptible materials/locations, and, if necessary, qualify swelling-resistant materials for LWR service.

The calculations results reported in the previous Milestone Reports [1-5] and some Monthly reports during this fiscal year have been done within the Standard Rate Theory (SRT) approach, that is the primary damage is represented by Frenkel pairs only, which allowed to clarify some issues related to the irradiation behavior of austenitic stainless steels at temperatures below 350°C. It has been shown that accounting residual gas and cascade production of vacancy loops are the most important findings, which allow predicting reasonable values of void density and swelling behavior presented in the last reports. However the results cannot be taken as fully correct because the framework used does not take into account an important observation, namely existence of so-called "incubation dose", which can be seen in Fig. 1 showing that the dose depends of swelling. The incubation dose is about 20 dpa at ~500°C and increases to ~ 50 dpa at 400°C. The incubation dose at temperature smaller below 400°C would be expected to be even larger. Note that accounting of the incubation dose within the SRT framework was done in an artificial way: it was assumed that there is no void nucleation during the incubation dose, which contradicts to numerous observations. In addition, within the SRT framework the nucleation of interstitial loops (SIA loops) was described via the reaction between the single interstitials is not correct. This is because production of SIA loops, similar to the vacancy loops, takes place during cooling down phase of displacement cascades. The SRT framework does not take into account one-dimensional diffusion of SIA mobile clusters, which are also produced by cascades. Accounting for all the differences means changing the SRT framework to that of the Production Bias one. The

calculation results obtained for the first time within the Production Bias framework are presented below.

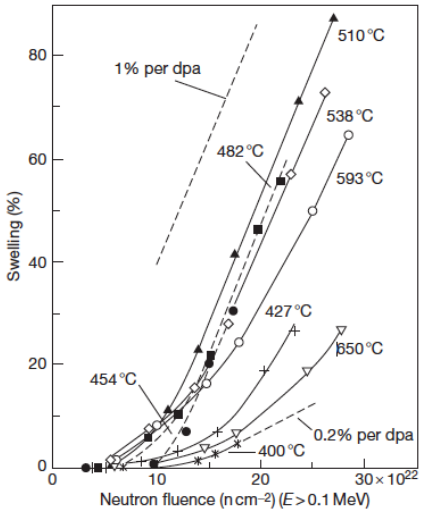

Fig. 1. Temperature dependence of swelling measured for AISI 316 stainless steels (Garner, Gelles, 1990).

2. Swelling accumulation in stainless steels

Existing database on swelling accumulation in stainless steels provide data in the range of < 60 dpa (see e.g. [6-8]). It has been founded that maximum swelling in this dose range and temperatures ~280-330°C does not exceed ~1%. However the void microstructures founded in [1-3] are quite different: the void density in [6,7] stays in the range of ~ 10^{20} - 10^{21} m^{-3} (the mean diameter ~10 - 20 nm) but they are extremely high, ~ 10^{23} m^{-3}, in [8] whereas the mean diameter is extremely small, ~ 1nm. Last swelling behavior is qualitatively different compare to that found in [6,7] and it will not be consider here since the reasons as to why such high void density takes place at temperatures when nucleation of high density of vacancy loops is expected, is not clear. The results of our study presented below are focused on data obtained in [7] since the data set presented in [7] covers the wide ranges of temperatures and doses. Indeed the temperature dependences of mean diameter, density of voids and swelling founded in [7] are presented in Figs. 2a, 2b and 2c. Figs. 2a-2c show that the maximum void density is ~4x10^{21} m^{-3}, mean diameter is less that 20 nm and maximum swelling is limited by ~1%.

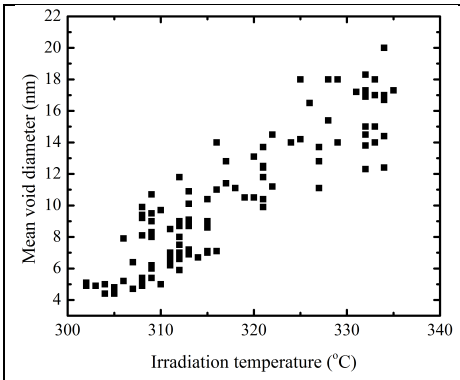

Fig.2a.Temperature dependence of the mean void diameter.

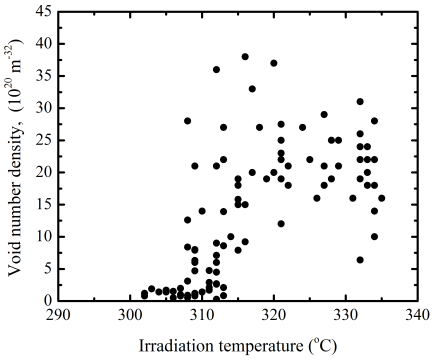

Fig.2b.Temperature dependence of the void concentration.

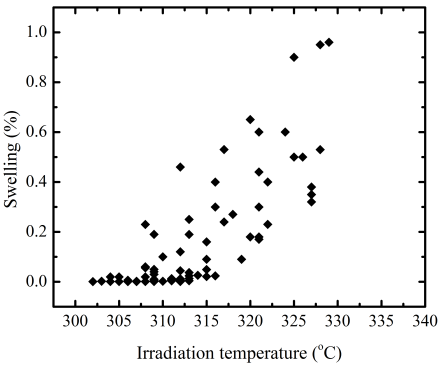

Fig.2c. Temperature dependence of void swelling.

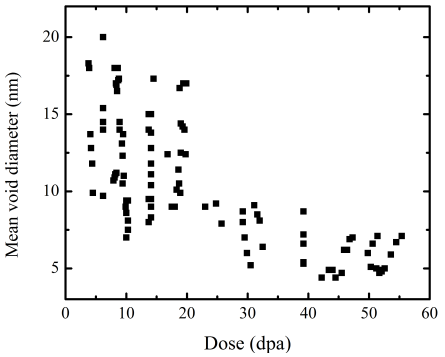

Fig.2d. Dose dependence of the mean void diameter.

In Fig. 2d the same data from [7] on the mean void diameter presented in Fig. 2a are presented as a function of dose. Concluding that the void evolution takes place in a way that the void size reaches saturation at the level between 5 and 20 nm depending on temperature: larger void sizes occur at higher temperature as it can be seen from a comparison of Figs. 2a and 2d. The void size saturation in a certain dose range is fully corresponded to a prediction followed from Production Bias Model [9,10]. Indeed, according to the PBM the swelling rate, $dS/d\phi$ ($S = 4\pi r^3 N/3$), is equal to the difference in the arrival rates of vacancies, single SIAs and one-dimensionally migrating SIAs clusters to voids:

$$\frac{dS}{d\phi} = \left[\left(\frac{4\pi r N \varepsilon_i^g}{4\pi r N + Z_v \rho} - \frac{\pi r^2 N \varepsilon_i^g}{\pi r^2 N + \pi \rho r_d / 2} \right) + \left(\frac{4\pi r N \left(1 - \varepsilon_i^g\right)}{4\pi r N + Z_v \rho} - \frac{4\pi r N \left(1 - \varepsilon_i^g\right)}{4\pi r N + Z_i \rho} \right) \right], \quad (1)$$

Unknown
Field Code Changed

where r and N are the mean void radius and Density, $\phi = (1-\varepsilon_r)\phi_{NRT}$ is the irradiation dose in dpa, which takes into account the fraction of defects that survive intra-cascade recombination (ε_r being the fraction of point defects recombining during the cooling stage of cascades), Z_v and Z_i are the capture efficiencies of edge dislocations for vacancies and single SIAs, respectively, and r_d is the dislocation capture radius for the SIA clusters. On the right-hand side of Equation (1), the swelling rate is divided into two terms proportional to the fractions of 1-D and 3-D migrating SIAs, respectively. If all SIAs were produced in the clustered form and migrated 1-D, then only the first term would exist and the swelling would cease when the void mean diameter reached the maximum value $d_{m0} = 2r_{m0} = 4\pi r_d / Z_v$ [11]. Note that taking the dislocation capture radius to be ~1 nm the magnitude of d_{m0} is ~ equal to $4\pi r_d \approx 13nm$. If, on the other hand, no 1-D migrating clusters are formed, as under electron irradiation, then only the second term would be present and unlimited void growth would be observed, with a rate proportional to the dislocation bias factor $B = Z_i / Z_v - 1$, which originates from a stronger interaction of single SIAs than vacancies with edge dislocations [12]. It is shown in [10] that the first term in Eq. (1) is responsible for void nucleation and its limited growth within a limited dose range due to random space distribution of voids whereas the second one is responsible for void size saturation at higher doses due to spatial correlations between voids and other defects, such as second-phase precipitates or dislocations, that provide shadowing of voids from the SIA clusters [10]. Possible scenarios of void evolution is shown in Fig. 3 showing that swelling saturation due to void growth cessation takes place when they are fully screened by other defects (see [10]).

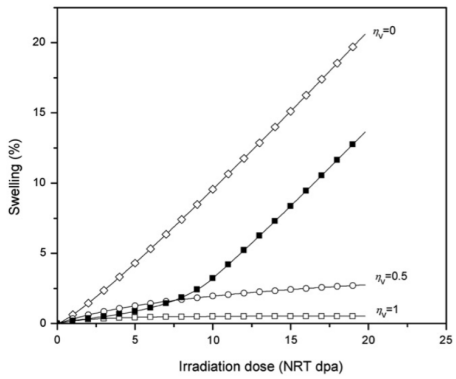

Fig. 3. Dependence of swelling on irradiation dose calculated using the above equation and different values of the correlation-screening factor of voids, η_v [10]. The curves with open cycles and filled squares have been calculated for correlations developing with irradiation dose.

Golubov, Stanislav I. 9/26/2016 10:38 AM
Formatted: Font:(Default) Times New Roman

Golubov, Stanislav I. 9/26/2016 10:35 AM
Deleted: (1)

Golubov, Stanislav I. 9/19/2016 12:36 PM
Formatted: Justified

Note that a non-random space distribution of voids was already observed by Cawthorne and Fulton [13] where void swelling was reported on for the first time. Examples of some detail observations of non-random space distribution of voids one can find e.g. in [14,15] are shown below

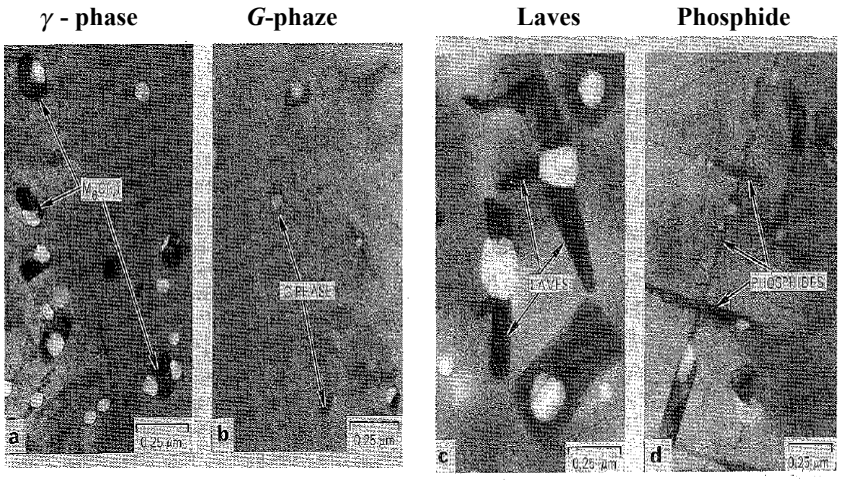

Fig. 4. Void association with the secondary phase particles during neutron irradiation of austenitic stainless steel [14].

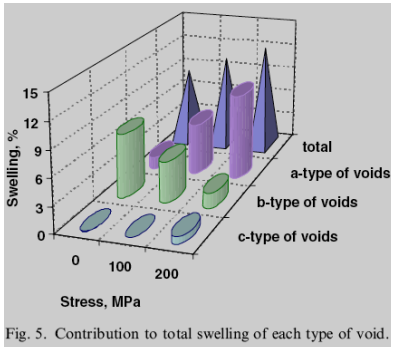

Fig. 5. Contribution to total swelling of each type of void.

Fig. 5. Contribution to total swelling of voids associated with the secondary phase particles and dislocations during neutron irradiation 20% cold-worked 16Cr15Ni2MoTiMnSi steel [15].

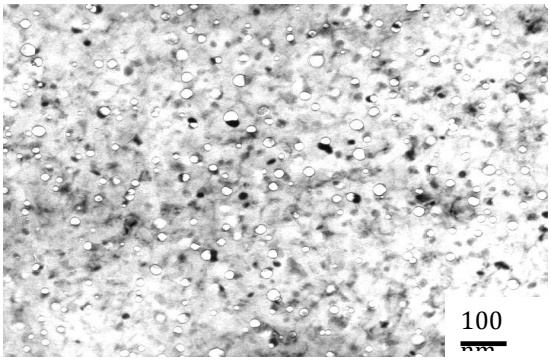

Fig. 6. Voids in the 12X18H9T steel after neutron irradiation at 324°C to 8.9 dpa [7].

In the case of the stainless steels under consideration, the association of voids with precipitates takes place already at the level of ~10 dpa that is shown in Fig. 6. Probably this may explain the higher magnitude of the mean size of voids at high temperatures shown in Fig. 2d since a deviation of void space distribution from random one has to increase with temperature increase.

In our view the data presented in Fig. 2d provide a strong evidence for validity of the Production Bias Model used in the present work.

3. Description of the Physical Model

The Radiation-Induced Microstructure Evolution (RIME) code developed by us [3] performs numerical integration of the master equations for the size-distributions of gas filled voids and vacancy and interstitial loops. The equations are coupled with equations for concentrations of the mobile species: single vacancies and-interstitial atoms and gas atoms migrating three dimensionally, and SIA clusters migrating one dimensionally. It also accounts evolution of the network dislocation density via interstitial loop transformation in the dislocation network and dislocation ageing via their climb. Both the network dislocations and faulted loops have a net bias for interstitials. Nucleation of voids takes place via interaction of vacancies between each other and gas atoms, whereas nucleation of vacancy and interstitial loops take place within cascades of displacement atoms. The fraction of the initially produced vacancies and interstitial loops, which are of the order of 10%, are used as fitting parameters. In addition cascade production of interstitial loops is assumed taking place during a limited irradiation dose that allows escaping of their unlimited nucleation (above the dose all the in-cascade produced interstitial loops are accounted as the mobile interstitial clusters.

A specially developed grouping scheme [16-18] and the double precision version of the Livermore solver for ordinary differential equations (DLSODE) [19] are used. The integration is performed in the (*x, m*) phase space, where *x* and *m* are the numbers of vacancies and gas atoms in a gas filled voids, and the *x* phase space, where *x* are the numbers of vacancies and interstitials in vacancy and interstitial loops, respectively. The output includes the dose dependence of the size distributions in the (*x, m*) and (*R, m*) phase spaces, where *R* is the void/loop radius, and integral characteristics of the microstructure, such as bubble and loop densities, bubble and loop mean sizes, swelling, and network dislocation density. The hardness or yield strength change associated with the microstructural evolution is calculated using a standard dispersed barrier-hardening model original form proposed by Orowan [20] as:

$$\sigma(t) = T\alpha Gb\sqrt{< d(t) > N(t)}\ , \qquad (2)$$

where *σ(t) is* the matrix hardening (strength increase), $< d(t) >$, $N(t)$ are the mean bubble diameter and density, *G* is the shear modulus, *b* is the magnitude of the Burgers vector, α is the so-called barrier strength which is a constant of the order of 0.1-0.5, and T=3.06 is the Taylor factor which relates the critical resolved shear stress to the change in the uniaxial yield strength [5]. Subsequent work has provided alternate formulations of Orowan's original model [21-24] and these revisions generally reduce the degree of predicted hardening. For simplicity, we here adopt Eq. (2) with a barrier strength $\alpha = 0.2$ and acknowledge that this may lead to an overestimate of the expected hardening. It is important to mention that comparisons of measured yield strength changes with the predictions of this dispersed-barrier model can be confounded by radiation-induced softening mechanisms such as precipitate dissolution. Note also that in the results presented below the barrier strength α = 0.2 is applied for all defects, i.e. voids, dislocation loops and dislocation network.

Unknown
Field Code Changed

Golubov, Stanislav I. 9/26/2016 10:38 AM
Formatted: Font:12 pt

Golubov, Stanislav I. 9/26/2016 10:35 AM
Deleted: (2)

4. Results of Simulations

Table 1 lists the nominal or baseline set of material and irradiation parameters employed in the results shown below. Parameters varied in the analysis include the pre-exponential factors of the mobile defects, the dislocation bias, the di-vacancy binding energy, the factions of cascade-produced vacancy and interstitial loops and clusters.

Table. 1. Nominal material and irradiation parameters

Parameter	Value	Description
T	275; 300; 325; 350	Temperature (°C)

Ω	1.14×10^{-29}	Atomic volume (m^3)
γ	1.65	Surface energy (J/m^2)
E_v^f	1.8	Vacancy formation energy (eV)
E_v^m	1.2	Vacancy migration energy (eV)
E_{He}^m	0.3	He migration energy (eV)
D_{v0}	5.0×10^{-6}	Vacancy pre-exponential coefficient (m^2/s)
D_{i0}	2.0×10^{-7}	Interstitial pre-exponential coefficient (m^2/s)
D_{g0}	2.0×10^{-7}	He pre-exponential coefficient (m^2/s)
ρ_d	2×10^{15}	Initial network dislocation density (m^{-2})
Z_v, Z_i	1.0, 1.04	Dislocation capture efficiencies
m / x_{max}	2	Maximum helium to vacancy ratio in bubbles
G_{NRT}	10^{-7}	NRT generation rate (dpa/s)
G_g	1.0	He generation rate (appm/dpa)
C_g	0.1, 1.0, 10.0	Residual gas concentration (appm)
ε_r	0.9	In-cascade recombination fraction
ε_v	0.1	Fraction of vacancies in vacancy loops
ε_i	0.1	Fraction of interstitials in immobile interstitial loops
ε_i^g	0.1	Fraction of interstitials in mobile interstitial loops
E_{2V}	0.3	Di-vacancy binding energy (eV)
R_g	1 m	Grain radius
$N_{v,max}$	3.6×10^{24}	Maximal density of vacancy loops and voids (m^{-3})
$N_{i,max}$	$N_i=N_{i0}e^{(E/kT)}$,	Maximal density of interstitial loops (m^{-3}), E~1 eV
ϕ_{inc}	50	Incubation dose, (dpa)
ϕ_{inc}	100, 150	Transient dose, (dpa)
ϕ_{max}	100	Maximal dose, (dpa)
G	80	Shear modulus (MPa)
b	2×10^{-10}	Burgers vector (nm)
T	3.06	Taylor factor
α	0.2	Barrier strength
Φ_I / Φ_T	50/100 (150)	Incubation/Transient dose (dpa)

Before calculation of swelling accumulation at LWRS relevant conditions our model and RIME code has been tested for the case of fast breeder reactor, which provided much

more data in the wide range of temperatures and doses presented in Fig. 1. The calculation has been done with taking into account that the duration of the incubation doses are equal to 20 and 50 dpa for 500 and 400^{0}C, respectively. Fig. 7 shows that our model and code excellently reproduce the experimental data for swelling accumulation with the nominal material parameters except the generation rate, which is ~ an order of magnitude high in the case of fast breeder reactor that provides a confidence that the new versions of our model and RIME code may provide a solid basis in prediction of swelling behavior at doses essentially higher than that provided now by experiment. The calculation results obtained with the nominal material parameters for temperatures and the generation rate relevant to LWRS conditions are presented below

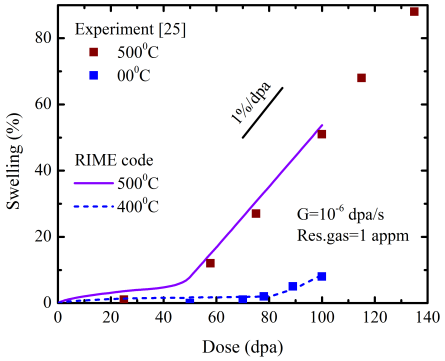

Fig. 7. Comparison of the dose dependence of swelling measured for AISI 316 stainless steels [25] and calculated with RIME code for fast reactor irradiations. Residual gas concentration is equal to 1 appm.

Dose dependence of swelling and the mean void diameter at 300^{0}C calculated with the nominal parameters are presented in Figs. 8 and 9. Fig. 8 shows that swelling accumulation predicted by the calculations is reasonably agree with the observation.

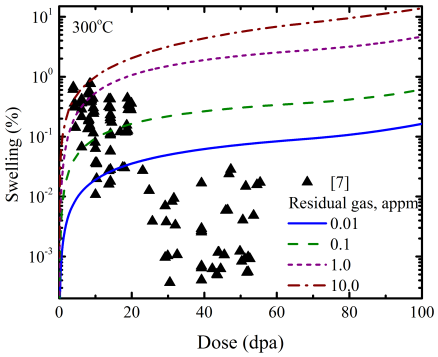

Fig. 8. Dose dependence of swelling calculated at 300^{0}C for different magnitudes of the residual gas

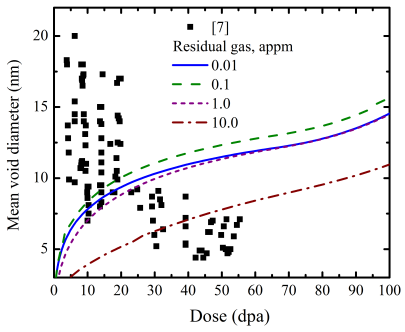

Fig. 9. Dose dependence of the mean void diameter calculated at 300^{0}C for different magnitudes of the residual gas

concentration.	concentration.

Moreover Fig. 9 shows that the mean void size does not changed significantly with an increase in residual gas concentration whereas swelling does it. This suggests that the level of swelling in the incubation regime is fully determined by void density which in turn is influenced by the residual gas concentration.

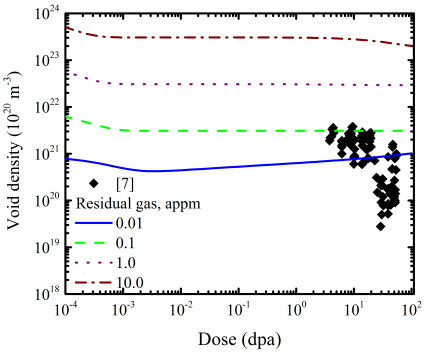

Fig. 10. Calculated dose dependence of void density at 300^{0}C for different residual gas concentration and this found in [7]

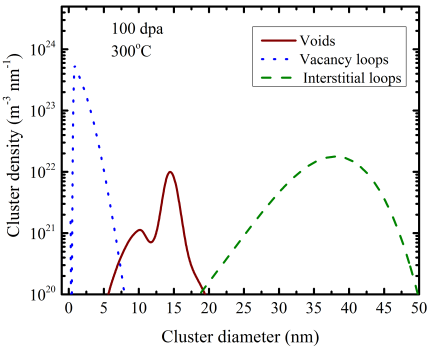

Fig. 11. Size distributions of voids and vacancy and interstitial loops after irradiation to 100 dpa at 300^{0}C at 1appm concentration of the residual gas.

The dose dependence of void density at 300^{0}C for different residual gas concentration is presented in Fig.10 showing that steady-state concentrations are built up at very low doses due to high vacancy super saturation. The calculated data obtained for the lowest residual gas concentrations of 0.01 and 0.1 appm are reasonably agree with the observations. The size distributions of voids and vacancy and interstitial loops after irradiation to 100 dpa at 300^{0}C at 1appm concentration of the residual gas are presented in Fig. 11. This shows that the density and sizes of the voids and loops are quite different: vacancy loops reach the highest density but with small size, due to their thermal instability. In contrast the size of interstitial loops is quite large because they are thermally stable and have a positive dislocation bias. The void size is not very high since void size increase requires accumulation a large amount of vacancies as the void radius increases proportional to $n_v^{1/3}$. Whereas $n_{v,i}^{1/2}$ for dislocation loops, where n_v, $n_{v,i}$ are the total number of defects in voids and loops.

Shearing of mobile defects for the case under consideration, i.e. when four different types of defects: voids, vacancy and interstitial loops and dislocations, is quite complicated. Illustrated in Figs. 12 and 13 are the dose dependence of the three-dimensionally sink strengths and one-dimensionally sink strengths of voids and vacancy and interstitial loops at 300^{0}C and the residual gas concentration equal to 1 appm are presented. In the case of three-dimensional reaction kinetics, Fig. 12, the vacancy loops provide the largest sink whereas in the case of one-dimensional reaction kinetics the interstitial loops provide the largest sink. Moreover the dose dependences of the different sink strengths are also quite

different: in three-dimensional case the sink strength of interstitial loops is decreased at high doses whereas in one-dimensional case the sink strength of vacancy loops is decreased at high doses. The dose dependences of void sink strengths are also quite different in the different reaction kinetics. Since the thermal stabilities of voids and vacancy dislocation loops is involved in the defect accumulations the sink strength dose dependences presented in Figs 12 and 13 they will be temperature dependent leading to temperature dependence of swelling. An example of it is presented in Fig. 14.

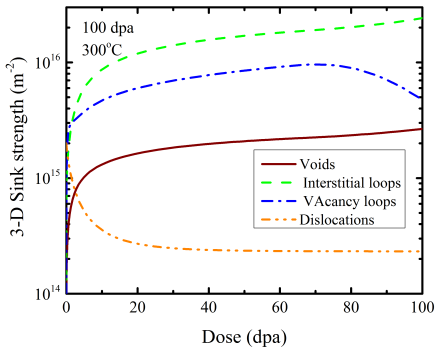

Fig. 12. Calculated dose dependence of the three-dimensionally sink strengths of voids and vacancy and interstitial loops at 300^{0}C and the residual gas concentration equal to 1 appm.

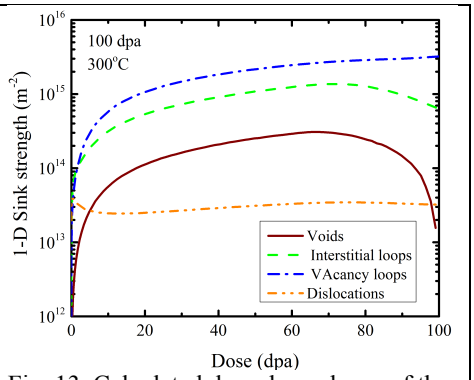

Fig. 13. Calculated dose dependence of the one-dimensionally sink strengths of voids and vacancy and interstitial loops at 300^{0}C and the residual gas concentration equal to 1 appm.

Dose dependences of swelling calculated for irradiation temperatures in the range 275-400^{0}C are presented in Fig. 14. Fig. 14 shows that the dose dependences in the range of 275-325^{0}C have similar shape and gradually increase with temperature. The dependences for temperatures 350 and 400^{0}C become slightly different: at 350^{0}C swelling becomes smaller than that for the low temperatures and becomes larger at the highest doses. At 400^{0}C the dose dependence became qualitatively different: in the dose range < 60 dpa swelling is saturated and starts rapidly increase at higher doses. Such a change in swelling accumulation takes place due to annealing of vacancy loops, which has a strong temperature effect.

The dose dependence of the strength increase calculated with Eq. (2) at 300^{0}C and residual gas concentration equal to 0.1appm is presented in Fig. 15. Fig. 15 shows that the strength increase become quite high already at very small doses that takes place due to the fast increase of the density of voids and dislocation loops. In contrast, its increase at higher doses, which is driven by an increase of the void and loop sizes, is quite slow. Note however that the dose dependence of the strength increase presented is quite preliminary because the barrier strength ($\alpha = 0.2$) in the present calculations is applied for all defects, i.e. voids, dislocation loops and dislocation network which may not be correct.

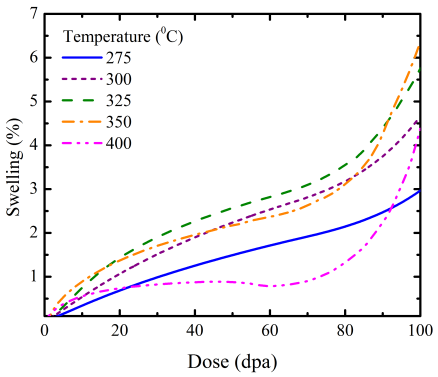

Fig. 14. Dose dependence of swelling calculated for different irradiation temperatures.

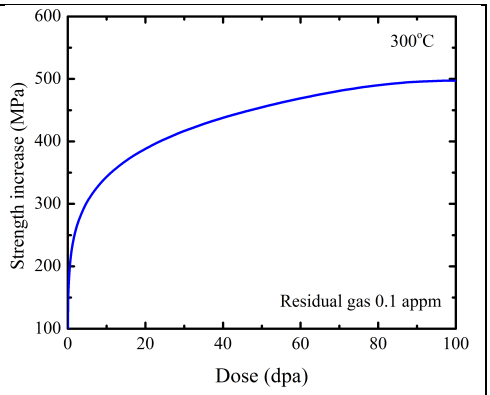

Fig. 15. Dose dependence of the strength increase at 300^{0}C calculated by use of Eq. 2 for residual gas concentration 0.1 appm.

4.0 Conclusions

A recently revised and improved mean-field reaction rate theory model and RIME code has been applied to investigate the potential for swelling of austenitic stainless steels at high doses under exposure conditions relevant to LWR internal components. The main part of the improvement is related to accounting all major properties of primary defect production taking place under neutron irradiation: cascade production of vacancy and interstitial faulted dislocation loops in addition to point defects and, that is vitally important, production of interstitial clusters migrating one-dimensionally. Accounting for these cascade properties transforms the reaction kinetics from pure three-dimensional to the mix of three and one-dimensional ones. It is shown that cascade nucleation of vacancy loops does effect void evolution but in a different way compare to that predicted by well known BEK model [26] where swelling cessation at low temperatures was attributed due to absent of void nucleation. In fact, as it is shown by calculations presented here, the void nucleation takes place due to existence of "production bias" whereas the void growth is suppressed as it is predicted by Eq. (1) due to the void random space distribution (see e.g. [9,10]).

With a given parameterization, the predictions of the model are reasonably consistent with the available microstructural data such as measurements in [7] of swelling, size and density of voids. Although the model predictions are sensitive to a range of material and irradiation parameters, our calculations suggest that swelling at temperature ~300^{0}C will

not increase more that several percent at a dose of ~100 dpa. However it could be higher at higher temperatures due to suppression of the vacancy loops and more effective association of voids with the secondary phase precipitates.

5.0 Future Work

The calculation results present here allow us to clarify the nature of so-called incubation period in swelling accumulation in accordance with what the modern theory predicted. Moreover RIME code demonstrated an ability to calculate simultaneous evolution of different type of defect such as voids, dislocation loops and dislocations is high accuracy. However the results achieved are quite preliminary due to variety reasons:

1. The set of parameters involved in the model is quite large but not all of them are known well
2. The mechanisms responsible for a duration of the transient regime in swelling accumulation are not developed
3. The mechanisms responsible for the transient period, i.e. when swelling accumulation is increased and may reach a critical value, required further development.

The theory [9,10] provide a qualitative explanation for the different stages of swelling accumulation but the real mechanisms responsible for them have never been investigated. This has to be done to make the model and RIME code to be able predicting damage accumulation in different structure materials relevant to LWRS project.

References

1. R. E. Stoller, A. V. Barashev, and S. I. Golubov, "Low-temperature Swelling in LWR Internal Components: Current Data and Modeling Assessment," ORNL/LTR-2012/390, September 2014, Oak Ridge National Laboratory, September 2012.
2. R. E. Stoller, A. V. Barashev, and S. I. Golubov, "The Influence of Helium on Low- temperature Swelling in LWR Internal Components," ORNL/LTR-2013/200, Oak Ridge National Laboratory, September 2013.
3. A. V. Barashev, and S. I. Golubov, R. E. Stoller, A Model of Radiation-induced Microstructural Evolution, ORNL/LTR-2014/487, Oak Ridge National Laboratory, September 2014.
4. R. E. Stoller, S. I. Golubov and A. V. Barashev, Low-temperature Swelling in LWR Internal Components: a Computational Assessment, 17th International Conference on Environmental Degradation of Materials in Nuclear Power Systems – Water Reactors August 9-12, 2015, Ottawa, Ontario, Canada.

5. R. E. Stoller, A. V. Barashev, and S. I. Golubov, Swelling In Light Water Reactor Internal Components: Insights from Computational Modeling, ORNL/LTR-2015/439, Oak Ridge National Laboratory, August 2015.
6. D.J. Edwards, F.A. Garner, B.A. Oliver and S.M. Bruemmer, Microstructural Evaluation of a Cold-Worked 316SS Baffle Bolt Irradiated in a Commercial PWR, Tenth International Conf. on Environmental degradation of materials in Nuclear power Systems-Water powers, Pacific Northwest National Laboratory, Richland, WA 99352.
7. Porollo, S. I., Konobeev, Yu. V., Dvoriashin, A. M., Krigan, V. M., and Garner, F. A., "Determination of the Lower Temperature Limit of Void Swelling of Stainless Steels at PWR-Relevant Displacement Rates", The Effects of Radiation on Materials, 21st International Symposium, ASTM STP1447, M. L. Grossbeck, T. R. Allen, R. G. Lott, and A. S. Kumar, Eds., ASTM International, West Conshohocken, PA, 2003.
8. Chung, H. M. "Assessment of void swelling in austenitic stainless steel core internals," NUREG/CR-6897, ANL-04/28, Argonne National Laboratory, December, 2004.
9. S.I. Golubov, A.V. Barashev, and R.E. Stoller (2012) Radiation Damage Theory. In: Konings R.J.M., (ed.) Comprehensive Nuclear Materials, volume 1, pp. 357-391, Amsterdam, 2012: Elsevier.
10. A.V. Barashev, S.I. Golubov, Unlimited damage accumulation in metallic materials under cascade-damage conditions Phil. Mag. 89, 2009, 2833-2860.
11. H. Trinkaus, B.N. Singh and A.J.E. Foreman, J. Nucl. Mater. 199 (1992) p.1.
12. G.W. Greenwood, A.J.E. Foreman and D.E. Rimmer, J. Nucl. Mater. 4 (1959) 305.
13. C. Cawthorne, and E. J. Fulton, "Voids in irradiated stainless steel," Nature 216 (1967) 575-576.
14. Pedraza, D. F.; Maziasz, P. J., Void-Precipitate Association During Neutron Irradiation of Austenitic Stainless Steel; In *Radiation-Induced Changes in Microstructure: 13th International Symposium (Part I), ASTM STP 955,* F.A. Garner, N.H. Packan, and, A.S. Kumar, Eds., American Society for Testing and Materials: Philadelphia, 1987, pp. 161-194.
15. I.A. Portnykh, A.V. Kozlov, V.L. Panchenko, V.M. Chernov, F.A. Garner, The mechanism of stress influence on swelling of 20% cold-worked 16Cr15Ni2MoTiMnSi steel, J. Nucl. Mater. 367–370 (2007) 925–929.

16. S.I. Golubov, A.M. Ovcharenko, A.V. Barashev, and B.N. Singh, "Grouping method for the approximate solution of a kinetic equation describing the evolution of point-defect clusters," Philos. Mag. A. 81 (2001) 643-658.
17. S.I. Golubov, R.E. Stoller, and S.J. Zinkle, "Nucleation and growth of helium-vacancy clusters in irradiated metals. Part. I. A group method for an approximate solution of two dimensional kinetic equations describing evolution of point defect clusters," Fusion materials semi-annual progress report for period ending December 31, 2002, DOE/ER- 0313/33, US Department of Energy, pp. 155-180.
18. S.I. Golubov, R.E. Stoller, and S.J. Zinkle, "Nucleation and growth of helium-vacancy clusters in irradiated metals. Part. I. A group method for an approximate solution of two dimensional kinetic equations describing evolution of point defect clusters," Fusion materials semi-annual progress report for period ending December 31, 2002, DOE/ER- 0313/33, US Department of Energy, pp. 155-180.
19. K. Radhakrishnan and A.C. Hindmarsh, "Description and use of LSODE, the Livermore Solver for Ordinary Differential Equations," UCRL-ID-113855, Lawrence Livermore National Laboratory, NASA Reference Publication 1327, 1993.
20. E. Orowan, in Internal Stresses in Metals and Alloys, The Institute of Metals, London, 1948, pp. 451-453.
21. A.L. Bement, Jr., in Strength of Metals and Alloys, Proceedings of Second International Conference., ASM International, Metals Park, OH, 1973, pp. 693-7288.
22. P. M. Kelly, Int. Metallurg. Rev. 18, 31 (1973).
23. U. F. Kocks, Mat. Sci. and Engr. 27 (1977) 291-298.
24. R. E. Stoller and S. J. Zinkle, J. Nucl. Mater, 283-287 (2000) 349-352.
25. F. Garner, D. Gelles, “Neutron-Induced Swelling of Commercial Alloys at Very high Exposers”, Effects of Radiation on Materials: 14 International Symposium (Vol. II), ASTM STP 1046, N.H. Packan, R.E. Stoller, and A.S. Kumar, Eds., American Society of Testing Materials, Philadelphia, 1990; pp. 673-683.
26. R. Bullough, B.L. Eyre, K. Krishan, Cascade damage effects on swelling of irradiated materials, Proc. R. Soc. London. A 346, 1975, 81-102.